Chronicles from the Frequency Domain:
Benefits & Applications of AC Thermal Modeling, Simulation & Measurement

B. Vermeersch[1], G. De Mey[1], J. Banaszczyk[1], A. Shakouri[2], K.A.A. Makinwa[3]

E-mail: **bjorn.vermeersch@elis.ugent.be**

[1] Electronics & Information Systems, Ghent University, Sint Pietersnieuwstraat 41, 9000 Gent, Belgium.

[2] Baskin School of Engineering, University of California at Santa Cruz, California USA.

[3] Electronic Instrumentation Lab, Delft University of Technology, The Netherlands.

Summary   *AC analysis, i.e. the study of sinusoidal regime, is not widespread in the field of thermal analysis of electronic devices. However, this technique, commonly used in other branches of electrical engineering, can be favorably adopted to thermal problems. The method involves the investigation of periodic oscillations of the temperature and heat flux induced by a sinusoidal power dissipation (with angular frequency $\omega = 2\pi f$). The thermal fields can be mathematically described using a complex phasor notation. A major role is played by the thermal impedance $Z_{th}(j\omega)$, i.e. the ratio of the temperature and power phasor in the junction.*
Thermal frequency domain analysis is directly applicable to components that are typically operated in pulsed mode, such as power electronics and electrothermal filters. More generically, the use of phasors often simplifies both analytical modeling and numerical simulation. Electrothermal analogies can be beneficially exploited as well, e.g. RC ladder networks can be elegantly analysed in the frequency domain. This has lead to the development of a transient fixed-angle heat spreading model. In addition, the Nyquist plot of $Z_{th}(j\omega)$ shows some interesting properties not revealed in the time domain. Such an impedance curve offers a compact yet complete thermal blueprint of the device and can be used for quality inspection purposes. Finally, AC measurements provide phase information, which acts as a sensitive heat detector hardly affected by calibration errors or noise. Frequency domain experiments also enable separation of Joule and Peltier effects. AC temperature fields on the IC surface can be visualised with high spatial resolution by means of CCD-based thermoreflectance. As an example, some results obtained with a novel heterodyne technique on thermoelectric microcoolers are presented.

1   Introduction and General Concept

The starting point for a frequency domain approach to thermal analysis is to assume that the power dissipated by the electronic device under study is purely sinusoidal. The frequency of the power oscillation is noted as f; the associated angular frequency is given by $\omega = 2\pi f$. We will limit ourselves to moderate temperature rises, i.e. a few tens of degrees above ambient, such that the thermal parameters can be reasonably considered as constant. In a thus linear system, the sinusoidal power induces periodic oscillations of the temperature and heat flux distributions, at the same frequency f.

The sinusoidal thermal fields can be efficiently represented by means of a complex phasor. By definition, a transient signal $x(t)$ is related to its associated phasor $X(j\omega)$ by: $x(t) = \mathrm{Re}[X(j\omega)\exp(j\omega t)]$ with $\mathrm{Re}[\cdot]$ the operator taking the real part and $j = \sqrt{-1}$ the complex unit.

It is interesting to normalise the temperature to the amount of total dissipated power, by taking the ratio $T(j\omega)/P(j\omega)$. When evaluated in the active junction, we obtain the thermal impedance $Z_{th}(j\omega)$. As one may expect, this quantity is nothing else than a generalisation of the steady state (DC) limit known as thermal resistance: $Z_{th}(j\omega \rightarrow 0) = R_{th}$. It turns out that the thermal impedance provides a powerful instrument for dynamic thermal characterisation of electronic devices. Additional details will be provided in section 4. Finally, it is worth mentioning that AC analysis can be considered as a particular case of Laplace transformation, namely an evaluation along the imaginary axis is performed: $s = j\omega$.

2   Direct Applications

Power Electronics

Periodic signals are commonly encountered in certain fields of technology. Power electronics, and IGBTs and diodes used in power conversion and traction applications in particular, are a major example. In these cases the active devices undergo rapid periodic cycling between on and off states, with pulse repetition frequencies that may exceed 100 kHz. Since the power signals and hence also the temperature fluctuations are periodic, it is almost a natural approach to perform the thermal analysis in the frequency domain. Investigation of the DC component and a couple of dominant harmonics can already provide a very decent assessment of the main features of the thermal behavior. Obviously, for a more detailed study, e.g. accurate determination of the peak temperature, an analysis over a much wider frequency spectrum is needed. Still, AC techniques may turn out to be faster than their time domain counterparts, since the latter require many time steps over the initial transients to finally capture the periodic regime.

Case Study: Electrothermal Filters

Another illustrative example is the analysis of an electrothermal filter (ETF). This component consists of a heater and a thermopile, i.e. a set of thermocouples connected in series, integrated on the same substrate. An ETF can be easily realised in standard CMOS technology. The typical structure is sketched in Fig. 1(a).
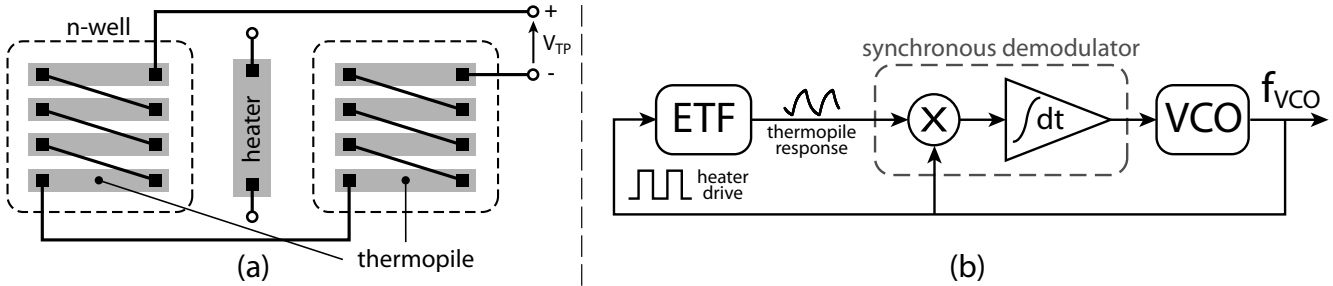

Figure 1: Electrothermal filter: (a) schematic layout; (b) application in temperature-to-frequency sensors.

The heater, driven by a square wave voltage, induces periodic heating in the substrate. The temperature fluctuations are sensed by the thermocouple junctions and translated back to the electrical domain. Due to the thermal inertia of the substrate, a frequency dependent phase shift and attenuation is introduced. Thus an ETF indeed filters the heater drive signal, but unlike conventional electrical filters, its characteristics are established in the thermal domain.

An electrothermal filter is typically not employed for filtering operations as such. Instead, it can be integrated into a frequency locked loop (FLL) as illustrated in Fig. 1(b). The loop settles at a frequency of the voltage controlled oscillator (VCO) f_0 for which the DC component of the integrator input becomes zero. Settling of the loop corresponds to a fixed phase shift in the ETF which, for a given device layout, essentially depends only on the diffusivity of the silicon substrate. As the temperature dependence of this parameter is very well known, the output frequency f_0 is, in turn, a well defined function of the absolute temperature as well. An ETF-based FLL hence enables realisation of highly reproducible temperature-to-frequency sensors using standard CMOS fabrication. Sensors with accuracy (3σ) better than 0.5°C over the military temperature range have been reported [1].

Further analysis shows that f_0 does not deviate far from the frequency where the ETF realises a 90 degrees phase delay, noted as f_{90}. For typical layouts a relation $f_0 \approx 0.95 f_{90}$ is observed. This means that adequate information on the thermal behavior can already be obtained from the study of a single sinusoidal component, namely the fundamental harmonic of the power dissipation in the heater. In such a case it is clearly advantageous to use AC analysis.

We have investigated the impact of several process parameters on the sensor performance by means of numerical 2-D simulation. The ETF is integrated on top of a lightly doped epi film. The rest of the substrate is strongly doped, resulting in a thermal conductivity about 30% smaller than that of the epi. The ETF is finally covered with a few microns of silicon oxide for passivation. It is worth mentioning that the oxide, despite being a poor thermal conductor ($k_{SiO_2} \approx 0.01 k_{Si}$), introduces a couple of additional degrees of phase delay. This may not seem much, but we note that every degree of extra phase shift roughly decreases the output frequency with 3 kHz, with f_0 in the order of 100 kHz.

Figure 2 shows the simulated phase shift of an actual ETF sample at room temperature. From the results we can estimate the FLL settling frequency as $f_0 \approx 0.95 \times 111 = 106$ kHz. This agrees very well with the output frequency of 103 kHz experimentally observed for the temperature sensor [2].

3   Modeling and Simulation Benefits

Even where no direct link with the frequency domain is present, namely for the many systems not operated under periodic conditions, AC thermal analysis can offer some inherent advantages. In the time domain, the generic heat equation for the transient temperature $T(\vec{r}, t)$ reads:

$$k\nabla^2 T(\vec{r}, t) - C_v \frac{\partial T(\vec{r}, t)}{\partial t} = -p(\vec{r}, t) \tag{1}$$

with k the thermal conductivity (W/m-K), $C_v = \rho C_p$ the volumetric heat capacity (J/m³K) and p the volumetric power density (W/m³). Transformation of (1) to the frequency domain yields, using phasor notation:

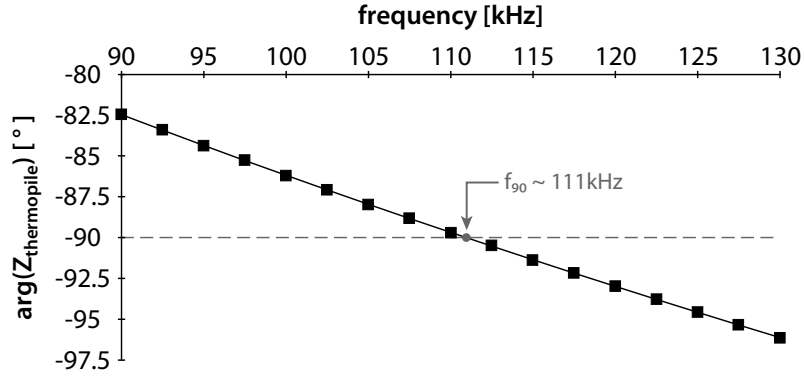$$k\nabla^2 T(\vec{r}) - j\omega C_v T(\vec{r}) = -p(\vec{r}) \tag{2}$$

Figure 2: ETF thermopile phase shift as function of frequency obtained by 2-D simulation.

We have thus reduced the heat equation from a partial differential equation to an ordinary differential equation. Both analytical and numerical solution is typically simpler for the latter. Once the AC solution is found, transient signals can be retrieved by means of inverse Fourier transformation techniques.

Another inherent AC benefit appears in the context of electrothermal analogies. It is well known that (quasi-)one-dimensional heat flows can be represented by an RC transmission line. Voltage and current along the line embody temperature and heat flow respectively. These distributed ladder networks can be elegantly analysed in the frequency domain because we can attribute a complex electrical impedance $\frac{1}{j\omega C}$ to the capacitors. One application is the treatment of thermal interface materials (TIMs) in numerical simulations. The material can be substituted by bounary conditions derived for an approximate equivalent thermal network. This reduces the system matrix while still accounting for the heat flow and energy storage in the interface.

Case Study: Transient Fixed-Angle Heat Spreading Model

We have also used the transmission line approach to develop a fixed-angle model suitable for dynamic thermal analysis of a rear-cooled substrate. Full details on the study can be found elsewhere [3]. We consider a heat source measuring $a \times a$ mounted on top of a substrate with thermal parameters k, C_v and thickness b. The bottom of the substrate is kept at ambient conditions (reference temperature $T = 0$). A fixed-angle model assumes that the heat from the source spreads into the substrate under a fixed angle ϕ. In other words, the heat is thought to be confined into a pyramidal body, with the isothermals and flux lines respectively parallel with and perpendicular to the heat source. A variety of such models is available in the literature since more than 40 years. However, the models are limited to steady state conditions: they only provide the thermal resistance R_{th}. We have proposed an extension to dynamic phenomena. The quasi 1-D heat flow that occurs under the fixed-angle assumption can be represented by an RC transmission line in which the line resistance and capacitance vary proportional to $\frac{1}{A(z)}$ and $A(z)$ respectively, with $A(z) = (a + 2z \tan \phi)^2$ the local cross-section area of the pyramidal body ($0 \leq z \leq b$). The thermal impedance 'felt' by the heat source is found to be:

$$\tilde{Z}_{th}(j\tilde{\omega}) = \frac{1}{2\lambda \tan \phi + \sqrt{j\tilde{\omega}} \cdot \mathrm{cotanh}(\sqrt{j\tilde{\omega}})} \tag{3}$$

in which the dimensionless substrate thickness $\lambda = \frac{b}{a}$ is introduced and both the impedance and frequency scales have been normalised:

$$\tilde{Z}_{th} = \frac{Z_{th}}{Z_0} \quad , \quad \tilde{\omega} = \frac{\omega}{\omega_0} \quad \text{with} \quad Z_0 = \frac{b}{ka^2} \quad , \quad \omega_0 = \frac{k}{C_v b^2} \tag{4}$$

Detailed comparison with the impedance obtained from fully analytical results for the actual 3-D thermal fields inside the substrate reveals that when an appropriate spreading angle $\phi = \phi_{\mathrm{opt}}(\lambda)$ is chosen, (3) stays within an error margin of 5% over the entire frequency range. This optimal angle is given by:

$$\phi_{\mathrm{opt}}(\lambda)[\text{degrees}] = \begin{cases} \lambda \leq 1 : & 5.86 \ln(\lambda) + 40.4 \\ \lambda \geq 1 : & 46.45 - 6.048 \, \lambda^{-0.969} \end{cases} \tag{5}$$

Appropriate processing of (3) provides the heating curve, i.e. the temperature response of the heat source to a 1 W power step. From this transient signal we can finally derive a thermal rise time, being the time needed for the temperature to

evolve from 10% to 90% of its final (steady state) value:

$$\tilde{t}_{rise} = 0.070 - 0.074 \, \frac{\lambda - 0.687}{\lambda + 0.687} \qquad , \qquad \tilde{t}_{rise} = \frac{t_{rise}}{t_0} \quad \text{with} \quad t_0 = \frac{2\pi \, C_v \, b^2}{k} \tag{6}$$

4 $Z_{th}(j\omega)$ as Thermal Blueprint

The thermal impedance can be calculated from analytical or numerical models directly in the frequency domain. It is also possible to measure it experimentally, namely by adequate Fourier processing of recorded heating or cooling curves. The resulting complex quantity is commonly represented in a Nyquist curve, i.e. a plot of $Im[Z_{th}(j\omega)]$ versus $Re[Z_{th}(j\omega)]$ with ω as a parameter. Figure 3(a) shows the measured thermal impedance curve for a packed power amplifier.
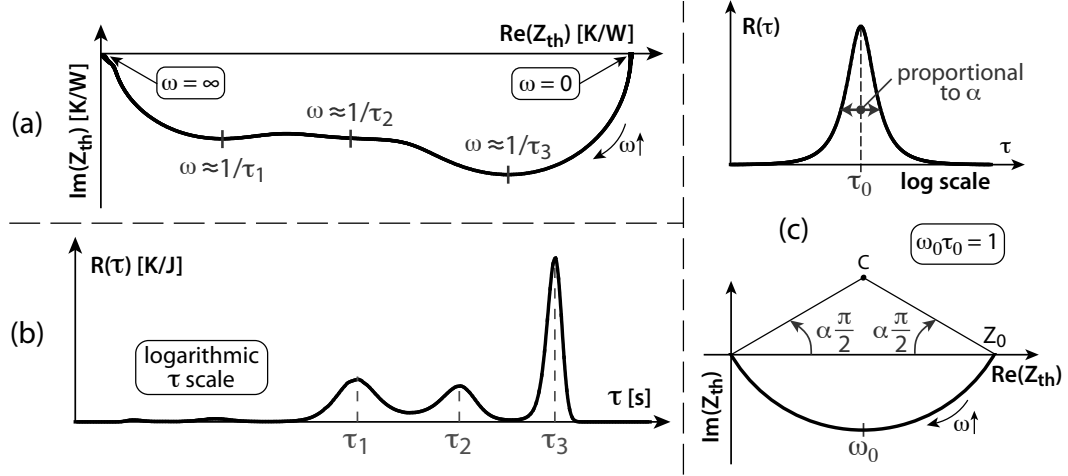

Figure 3: Exemplary thermal measurement: (a) Nyquist thermal impedance plot; (b) corresponding thermal time constant spectrum; (c) Fuoss-Kirkwood time constant distribution leading to circular impedance arc.

As published elsewhere [4] we have observed both theoretically and experimentally that in many cases the Nyquist plot of $Z_{th}(j\omega)$ is composed of a limited number $(2 \leq N \leq 5)$ of circular arcs. Since such an arc is entirely determined by 3 parameters, the impedance curve can be fully characterised with a limited set of data as well. Remind that $Z_{th}(j\omega)$ provides a complete, systematic description of the dynamic thermal behavior: if it is known over a sufficiently wide frequency range we are able to calculate the transient temperature for any arbitrary power dissipation. Therefore, the Nyquist plot of the thermal impedance can be considered as a compact thermal blueprint of the device.

The observed circular arcs are strongly related to the underlying time constants of the system, shown in Fig. 3(b). A thermal transient in the step response characterised by a single discrete time constant τ gives rise to a semicircle in the Nyquist impedance plot, i.e. with center on the real axis, and with central frequency $\omega = \frac{1}{\tau}$. In practice, however, the thermal impedance is the superposition of arcs having their center above the real axis. Mathematically this can be expressed as:

$$Z_{th}(j\omega) = \sum_{n=1}^{N} \frac{Z_n}{1 + (j\omega\tau_n)^{1-\alpha_n}} \qquad , \qquad 2 \leq N \leq 5 \tag{7}$$

Z_n is the chord intersected with the real axis, τ_n^{-1} the central frequency and α_n a parameter determining the deviation between the center point and the real axis, as illustrated in Fig. 3(c). Fuoss and Kirkwood [5] have proved earlier, in the context of complex dielectric constants, that a circular arc with its center above the real axis corresponds to a certain continuous distribution of time constants around the dominant constant τ_n. The width of the distribution is related to the parameter α_n. When the dominant time constants τ_n are sufficiently separated, the associated circular arcs can be distinguished individually. In our example this is the case for τ_3 and, although less pronounced, for τ_1 (see Fig. 3).

The decomposition (7) can offer practical applications, e.g. for quality monitoring. A test scheme could consist of turning measured heating curves into small sets of (Z_n, τ_n, α_n) values. A significant change in this set for a certain sample may signal anomalous behavior, while the affected circular arcs provide qualitative clues on how far from the junction a potential problem occurs.

5   AC Thermal Measurements

In simple terms, experimental thermal analysis for electronics applications consists of recording the transient temperature of the IC. The gathered information can range from a single-point quantification in the active junction to a wide spatial 2-D distribution. Typically three major ways of temperature measurements can be considered, namely physically contacting (e.g. scanning thermal microscopy), optical (e.g. thermoreflectance) and electrical methods (e.g. embedded sensors) [6]. Many of these techniques are applicable to frequency domain operation, although the practical suitability and attainable bandwith may largely vary. The main concept of an AC measurement is to supply the DUT with a periodic (usually purely sinusoidal) voltage or current and use a lock-in scheme at the detector side to tune into the desired harmonic.

A major generic advantage of AC methods is that they are more robust to noise as opposed to their time-domain counterparts [6]. In addition, both amplitude and phase information is provided. The latter can be shown to be far less influenced by system noise and calibration errors. This makes thermal phase recordings an interesting way of detecting weak heating signals (i.e. with temperature rises close to the measurement resolution).

Case Study: Heterodyne Thermoreflectance of Thermoelectric Microcoolers

Another additional benefit of AC measurements can be employed in the study of thermoelectric microcoolers. When supplied with a suitable current, these devices can achieve net subambient temperatures, owing to the dominance of Peltier cooling over Joule heating [7]. It has been demonstrated both theoretically and experimentally that the temperature distribution (relative to ambient) inside a microcooler can be written as:

$$T_{\text{cooler}}(\vec{r}) = a(\vec{r})I + b(\vec{r})I^2 \qquad a < 0 \text{ (Peltier)}, \ b > 0 \text{ (Joule)} \ ; \ I \text{ is the supply current} \tag{8}$$

When supplying a sinusoidal current $I(t) = I_0 \cos(2\pi ft)$ to the cooler, we obtain:

$$T_{\text{cooler}}(\vec{r}) = \frac{1}{2}b(\vec{r})I_0^2 + a(\vec{r})I_0 \cos(2\pi ft) + \frac{1}{2}b(\vec{r})I_0^2 \cos(4\pi ft) \tag{9}$$

The Peltier and Joule effects manifest themselves at different harmonics, and hence AC measurements allow to study them completely independently. Establishing lock-in on the appropriate frequency will capture the desired component. With time domain techniques this is not possible as there the superposition of both effects will be observed.

The experimental analysis of microcoolers and other devices can be carried out by means of thermoreflectance. This technique is based on the weak but detectable temperature dependence of the optical reflectivity of the IC surface. The effect is quantified by the thermoreflectance coefficient C_{TR}, which varies among different materials and strongly depends on the illumination wavelength. Figure 4(a) illustrates the general principle. Further details on the developed heterodyne methodology and according image processing, required to establish the lock-in for AC operation, are omitted here but will be presented elsewhere. Note that a miscalibration of C_{TR} will directly alter the extracted temperature amplitude, whereas the phase is left unaffected.

We have investigated the microcooler depicted in Fig. 4(b) biased with a 1 kHz sinusoidal current with amplitude of 47, 71 and 95 mA. The obtained thermal amplitude and phase images for first and second harmonic (Peltier and Joule effect respectively) are presented in Fig. 4(c). As expected, we observe that the amplitude of both harmonics gets larger as the magnitude of the supply current is increased, while the phase values remain virtually unchanged. The phase images simply get more pronounced for higher biases because the stronger heating signals are less influenced by noise. In addition, we can see that the Peltier component is clearly dominant over the Joule effect. In other words, the device is able to achieve net cooling over the considered current supply range. Finally, we noticed that the phase difference between first and second harmonic, relative to a common reference, systematically amounts to about 180 degrees. This can be explained by the different sign of a and b in (8).

6   Conclusions

We have reviewed the concept of thermal AC analysis, and briefly pointed out some areas where it has direct applications. Then an overview was given about how a frequency domain and phasor approach can be of great assistance for the thermal analysis of electronic systems in a general context. The generic importance of the thermal impedance $Z_{th}(j\omega)$, and its Nyquist plot in particular, were underlined. Benefits of a frequency domain approach to theoretical modeling, numerical simulation and experimental measurements were mentioned, and illustrated by practical case studies.
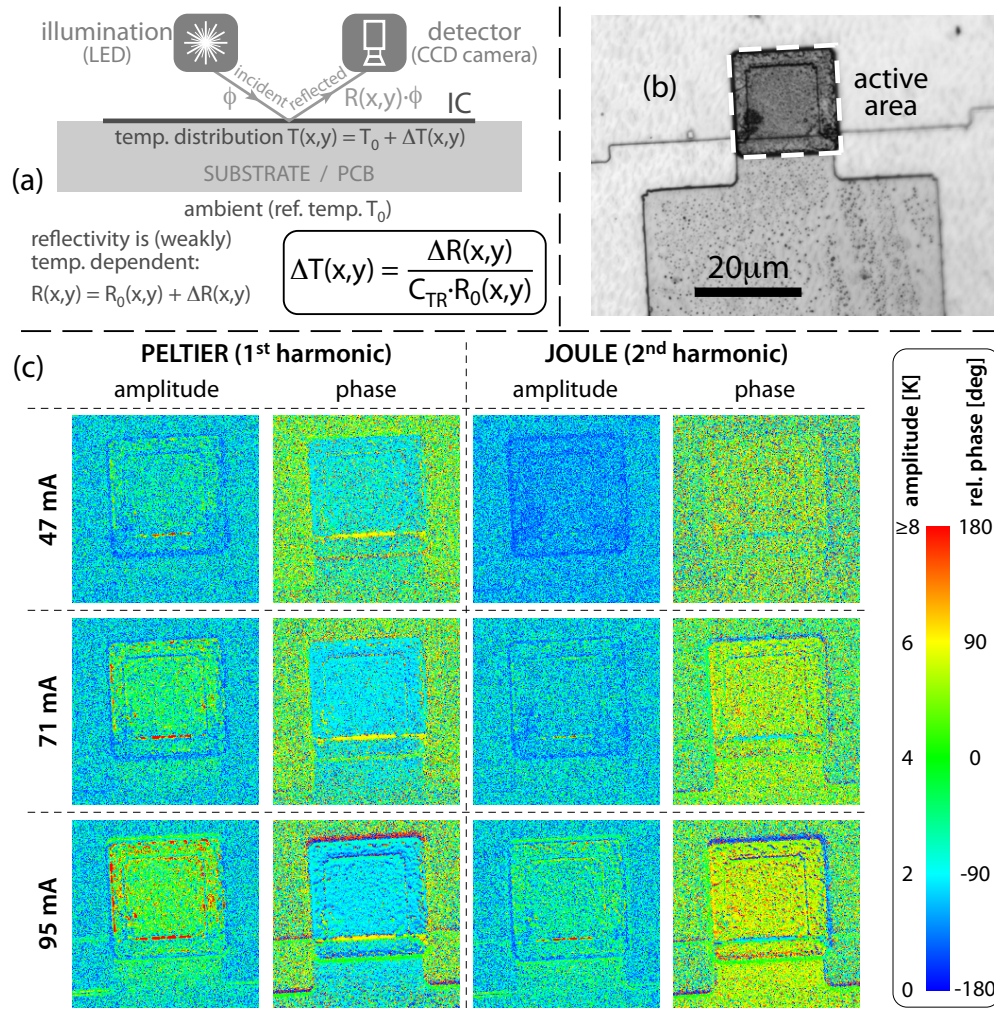
Figure 4: AC thermal imaging of a microcooler: (a) principle of thermoreflectance; (b) DUT; (c) obtained images at 1 kHz current biases.

7 Acknowledgements

References

[1] C.P.L. van Vroonhoven, K.A.A. Makinwa. A CMOS temperature-to-digital converter with an inaccuracy of $\pm 0.5^\circ$C (3σ) from -55 to 125°C. In *Proceedings of the IEEE International Solid-State Circuits Conference (ISSCC), San Francisco, California USA*, pp. 576–577, 2008.

[2] C. Zhang, K.A.A. Makinwa. Interface electronics for a CMOS electrothermal frequency-locked-loop. *IEEE Journal of Solid-State Circuits* **43**(7):1603–1608, 2008.

[3] B. Vermeersch, G. De Mey. A fixed-angle dynamic heat spreading model for (an)isotropic rear-cooled substrates. *Transactions of the ASME - Journal of Heat Transfer* **130**(12):121301/1–9, 2008.

[4] P. Kawka, G. De Mey, B. Vermeersch. Thermal characterization of electronic packages using the Nyquist plot of the thermal impedance. *IEEE Transactions on Components and Packaging Technologies* **30**(4):660–665, 2007.

[5] R. Fuoss, J. Kirkwood. Electrical properties of solids: Dipole moments in polyvinyl chloride diphenyl systems. *Journal of the American Chemical Society* **63**:385–394, 1941.

[6] J. Altet, W. Claeys, S. Dilhaire, A. Rubio. Dynamic surface temperature measurements in ICs. *Proc. of the IEEE* **94**(8):1519–1533, 2006.

[7] A. Shakouri. Nanoscale thermal transport and microrefrigerators on a chip. *Proceedings of the IEEE* **94**(8):1613–1638, 2006.